The role of the N-terminal domain in dimerization and nucleocytoplasmic shuttling of latent STAT3

The role of the N-terminal domain in dimerization and nucleocytoplasmic shuttling of latent STAT3

Michael Vogt[1], Tamas Domoszlai[1], Dzina Kleshchanok[2], Swen Lehmann[2], Anne Schmitt[1], Valeria Poli[3], Walter Richtering[2], Gerhard Müller-Newen[1#]

[1] Institute of Biochemistry and Molecular Biology, Medical School, RWTH Aachen University, Aachen, Germany

[2] Physical Chemistry, RWTH Aachen University, Aachen, Germany

[3] Department of Genetics, Biology and Biochemistry, Molecular Biotechnology Center, University of Turin, Torino, Italy

[#] Corresponding author:

Dr. Gerhard Müller-Newen

Institut für Biochemie und Molekularbiologie

Universitätsklinikum RWTH Aachen

Pauwelsstraße 30

52057 Aachen

Germany

Fon: ++49 241 80 88860

Fax: ++49 241 80 82428

e-mail: mueller-newen@rwth-aachen.de

Short title:

Dimerization and shuttling of STAT3

Keywords:

STAT3, dimerization, nucleocytoplasmic shuttling, confocal microscopy, dual-focus FCS

Summary

STAT3 is an important transcription factor involved in immunity and cancer. In response to cytokine stimulation STAT3 becomes phosphorylated on a single tyrosine residue. Tyrosine-phosphorylated STAT3 accumulates in the nucleus, binds to specific DNA response elements and induces gene expression. Unphosphorylated, latent STAT3 shuttles constitutively between cytoplasm and nucleus. We analyzed the importance of previously identified putative NLS and NES sequences for nucleocytoplasmic shuttling of latent STAT3 using STAT3-deficient cells reconstituted with fluorescently labelled STAT3 mutants. Mutation of a putative NLS or NES sequence did not impair nucleocytoplasmic shuttling of latent STAT3. We were also interested in the structural requirements for dimerization of unphosphorylated STAT3 and its relevance for nucleocytoplasmic shuttling. By native gel electrophoresis and dual-focus fluorescence correlation spectroscopy (2f-FCS) we identified the N-terminal domain (aa 1-125) to be essential for formation of unphosphorylated STAT3 dimers but not for assembly of tyrosine-phosphorylated STAT3 dimers. In resting cells the monomeric N-terminal deletion mutant (STAT3-ΔNT) shuttles faster between cytoplasm and nucleus than STAT3 wildtype indicating that dimer formation is not required for nucleocytoplasmic shuttling of latent STAT3. STAT3-ΔNT becomes phosphorylated and dimerizes in response to IL-6 stimulation but surprisingly does not accumulate in the nucleus. These results highlight the importance of the N-terminal domain in the formation of unphosphorylated STAT3 dimers and nuclear accumulation of STAT3 upon phosphorylation.

Introduction

The Jak/STAT signaling pathway is utilized by many cytokines and growth factors to rapidly transmit the signal from membrane bound receptors to the nucleus. The membrane-proximal cytoplasmic part of cytokine receptors is associated with Janus tyrosine kinases (Jaks). Upon activation by the ligand the Jaks phosphorylate cytoplasmic tyrosine residues of the cytokine receptors. These phosphotyrosine residues serve as docking sites for signaling molecules with an SH2 domain such as signal transducer and activator of transcription (STAT) transcription factors. STATs are recruited to the receptor and become phosphorylated on a single tyrosine residue by the Jaks. Phosphorylated STATs dimerize by reciprocal phosphotyrosine/SH2 domain interactions and translocate into the nucleus where they induce target genes (Levy and Darnell, 2002).

This canonical view of Jak/STAT signaling has been refined with regard to dimerization and nuclear translocation of STAT transcription factors. It has been firmly established that many if not all STAT proteins exist as preformed dimers in the absence of the activating tyrosine phosphorylation (Braunstein et al., 2003). However, the molecular interfaces that drive dimerization differ between individual STATs. In this respect STAT1 has been most thoroughly investigated (Mao et al., 2005). All STAT proteins are built up similarly. They consist of an N-terminal domain, a coiled-coil domain, the DNA-binding domain, a linker domain, a SH2 domain and finally the transactivation domain (see Fig. 2A). A STAT protein lacking the N-terminal domain and the C-terminal transactivation domain is often referred to as “core fragment”. Dimerization of unphosphorylated STAT1 is mediated by homotypic interactions of the N-terminal domains and reciprocal interactions of the core fragment resulting in an anti-parallel orientation (Mao et al., 2005). Also STAT3 is a dimeric protein in the absence of phosphorylation (Haan et al., 2000). While the core fragment of STAT1 contributes to dimerization the core fragment of STAT3 is a monomeric protein (Ren et al.,

2008). Thus, the N-terminal domain or the transactivation domain must be involved in the formation of unphosphorylated STAT3 dimers.

STATs are often described as latent cytoplasmic transcription factors that enter the nucleus in response to tyrosine phosphorylation. It is true that tyrosine phosphorylation of STATs leads to their nuclear accumulation. However, non-phosphorylated STATs are also able to enter the nucleus. They shuttle permanently between the cytoplasm and the nucleus resulting in a steady-state of high cytoplasmic and low nuclear STAT concentrations (Meyer and Vinkemeier, 2004). This nucleocytoplasmic shuttling of latent STATs is amazingly fast for e.g. STAT2 (Frahm et al., 2006) but quite slow for STAT3 (Pranada et al., 2004).

Among the seven mammalian STAT proteins (STAT1, 2, 3, 4, 5A, 5B, 6) STAT3 has the most pleiotropic functions (Levy and Lee, 2002). Its knockout leads to early embryonic lethality pointing to a role of STAT3 in embryonic development. In the adult STAT3 is an important transcription factor in immunity and inflammation. Dysregulated STAT3 activation is implicated in chronic inflammation and cancer (Yu and Jove, 2004). In this study we investigate the structural requirements for dimerization and nucleocytoplasmic shuttling of latent STAT3.

Results

1. Analysis of nucleocytoplasmic shuttling of STAT3 using the STAT3-CY construct.

For the analysis of nucleocytoplasmic shuttling we generated a STAT3 construct termed STAT3-CY that is C-terminally tagged with the cyan (CFP) and yellow fluorescent protein (YFP). Using the 514 nm laser of a confocal microscope YFP can be selectively bleached without damaging CFP (Fig. 1A). A shuttling assay in living cells has been worked out that is based on the cytoplasmic bleaching of YFP and detection of YFP and CFP fluorescence in cytoplasmic and nuclear regions of interests (ROIs). A decrease of nuclear YFP fluorescence is indicative for shuttling while the CFP fluorescence serves as an internal standard (Fig. 1B). Using this assay nucleocytoplasmic shuttling of latent STAT3 (Pranada et al., 2004) as well as persistently activated STAT3 (Herrmann et al., 2007) has been established.

The subcellular distribution of endogenous STAT3 and ectopically expressed STAT3-CY in murine embryonic fibroblasts (MEF) was compared (Fig. 1C). MEF with floxed STAT3 alleles ($MEF^{fl/fl}$) and MEF lacking STAT3 ($MEF^{\Delta/\Delta}$) were analyzed by immunofluorescence using a STAT3 antibody. In non-stimulated cells endogenous STAT3 is preferentially located in the cytoplasm but also nuclear STAT3 is detectable. Upon IL-6 stimulation the distribution is inverted with most of the STAT3 appearing in the nucleus and low amounts remaining in the cytoplasm (Fig. 1C, upper panel). $MEF^{\Delta/\Delta}$ were analyzed under identical settings to control specificity of the staining. Only a weak background signal was detectable (Fig. 1C, middle panel). The subcellular distribution of STAT3-CY in stably transfected $MEF^{\Delta/\Delta}$ and endogenous STAT3 in $MEF^{fl/fl}$ is comparable before as well as after stimulation (Fig. 1C, compare upper and lower panels). Thus, the CY-tag has no major influence on the subcellular distribution of STAT3.

2. Nucleocytoplasmic shuttling of putative NLS and NES mutants of STAT3

$MEF^{\Delta/\Delta}$ were stably transfected with STAT3-CY mutants to analyze the importance of putative NLS and NES sequences for nucleocytoplasmic shuttling (Fig. 2A). Lysates of these cells were prepared before and after IL-6 stimulation and analyzed for STAT3 expression and phosphorylation by immunoblotting (Fig. 2B). STAT3-ΔNLS-CY and STAT3-ΔNES-CY are phosphorylated on tyrosine 705 in response to IL-6 stimulation as are STAT3-CY in $MEF^{\Delta/\Delta}$ and endogenous STAT3 in $MEF^{fl/fl}$. STAT3-CY and the mutants show the expected apparent molecular mass of 145 kDa.

The subcellular distribution of the mutants was analyzed by confocal microscopy. In non-stimulated cells the distribution of STAT3-ΔNLS-CY is indistinguishable from STAT3-CY (Fig. 2C, upper and middle panels). However, upon phosphorylation STAT3-ΔNLS-CY does not accumulate in the nucleus. Compared to wild-type the distribution of STAT3-ΔNES-CY in non-stimulated cells is shifted to the nucleus. STAT3-ΔNES-CY responds to IL-6 stimulation with nuclear accumulation (Fig. 2C, lower panel). Thus, the STAT3 mutants double labelled with CFP and YFP behave as previously reported for the single-tagged proteins (Bhattacharya and Schindler, 2003; Ma et al., 2003).

The dynamic behaviour of the NLS- and NES-mutants was analyzed in the shuttling assay described above. For clarity, in the diagrams in Fig. 3 the YFP fluorescence in the cytoplasmic and nuclear ROIs but not the CFP fluorescence is depicted. Only those experiments were evaluated in which the CFP fluorescence in the nuclear ROI did not change during the measurement. Comparison of STAT3-CY (Fig. 3A) and STAT3-ΔNLS-CY (Fig. 3B) revealed that mutation of the putative NLS sequence of STAT3 does not have any impact on nucleocytoplasmic shuttling. STAT3-ΔNES-CY shuttles also between the cytoplasm and the nucleus. Unexpectedly, the rate of nucleocytoplasmic shuttling is even increased as indicated by the more rapid decrease of nuclear YFP fluorescence in response to cytoplasmic

bleaching. Fig. 3D shows an important control experiment proving that data recording alone does not contribute to any significant bleaching of the fluorophores. Thus, previously identified putative NLS- and NES-sequences of STAT3 are not required for nucleocytoplasmic shuttling of latent STAT3.

3. Dimerization of latent STAT3-CY analyzed by native gel electrophoresis

It has been firmly established that STAT3 and other STAT proteins form dimers in the absence of tyrosine phosphorylation (Braunstein et al., 2003; Haan et al., 2000). To assess the importance of dimerization for the nucleocytoplasmic shuttling of latent STAT3 we wanted to compare the shuttling of wild-type and monomeric mutants of STAT3. As outlined in the introduction based on structural investigations of STAT1 (Mao et al., 2005) and STAT3 (Ren et al., 2008) the N-terminal domain of STAT3 might be essential for dimerization.

To test the above hypothesis a deletion mutant of STAT3-CY lacking the N-terminal domain of STAT3 (STAT3-ΔNT-CY) was generated. Another mutant with two amino acid exchanged in the N-terminal domain was designed in analogy to a dimerization-deficient STAT1 mutant (STAT3-VL-CY, Fig. 4A). Lysates of stably transfected $MEF^{\Delta/\Delta}$ were analyzed by immunoblotting (Fig. 4B). Both mutants are tyrosine-phosphorylated in response to stimulation with IL-6. The counterstaining of STAT3 revealed the expected increased electrophoretic mobility of the deletion mutant STAT3-ΔNT-CY compared to STAT3-VL-CY.

In a first approach, the native molecular masses of the different STAT3-CY constructs were compared by blue-native PAGE (bnPAGE) of cellular lysates prepared under mild detergent conditions. After electrophoresis the gel was analyzed with a fluorescence scanner visualizing only the fluorescently labelled proteins (Fig. 4 C). Therefore, lysates of non-transfected $MEF^{fl/fl}$ display no signals. Lysates of non-stimulated $MEF^{\Delta/\Delta}$ expressing STAT3-CY show two bands, one representing the STAT3-CY monomer, the other representing the dimer.

Interestingly the dimer/monomer ratio does not change much upon stimulation. In contrast, non-phosphorylated STAT3-ΔNT-CY is a strictly monomeric protein. However, upon stimulation a fraction of dimers is generated. Dimerization of STAT3-VL-CY seems to be affected to some extend by the point mutations but is not abolished.

4. Dimerization of latent STAT3-eGFP analyzed by fluorescence correlation spectroscopy

Dimerization of STAT3 and STAT3-ΔNT was further analyzed by the recently established technique of dual-focus fluorescence correlations spectroscopy (2f-FCS). The basic concept of 2f-FCS is to use two laterally shifted and overlapping foci with a fixed and a well-known distance serving as an external ruler during the experiment. By measuring the autocorrelation function (ACF) from each foci and the dual-focus cross-correlation function (CCF) between both foci and analyzing these functions one can calculate the absolute values of the diffusion coefficient without further referencing or calibration (Dertinger et al., 2007; Müller et al., 2008).

For this purpose eGFP-labelled constructs were generated. COS-7 cells were transiently transfected with STAT3-eGFP, STAT3-ΔNT-eGFP and eGFP as a control. Lysates of these cells were prepared and analyzed by 2f-FCS. A representative autocorrelation function of each construct is shown in Fig. 5. Evaluation of the autocorrelation function of eGFP (Fig. 5A) by a one component fitting model resulted in a diffusion coefficient of $1.03 \pm 0.04 \times 10^{-6}$ cm^2/s that is in good agreement with published data (Kim and Schwille, 2003). An equivalent evaluation of the autocorrelation functions of STAT3-eGFP (Fig. 5B) and STAT3-ΔNT-eGFP (Fig. 5C) resulted in diffusion coefficients of 0.54 ± 0.08 and $0.7 \pm 0.03 \times 10^{-6}$ cm^2/s, respectively. From the diffusion coefficients the hydrodynamic radii according to the Stokes-Einstein relation can be obtained. In addition, the molecular masses of the STAT3 proteins were calculated based on the diffusion coefficient and the known molecular mass of eGFP (Table 1). The resulting molecular mass of STAT3-ΔNT-eGFP (88 ± 11 kDa) is in good

agreement with the predicted molecular mass of the STAT3-ΔNT-eGFP monomer (99 kDa). The apparent molecular mass of STAT3-eGFP (216 ± 99 kDa) fits with the predicted molecular mass of a STAT3-eGFP dimer (236 kDa). It was not possible do discriminate between a monomeric and a dimeric fraction of STAT3-eGFP due to limitations of the method. However, the high standard deviations in the measurements of STAT3-eGFP might be a consequence of a mixed population of monomers and dimers. Taken together, while STAT3-eGFP forms dimers the deletion of the N-terminal domain results in a purely monomeric population in resting cells.

5. Nucleocytoplasmic shuttling of monomeric STAT3

The subcellular distribution of STAT3-CY, STAT3-ΔNT-CY and STAT3-VL-CY in $MEF^{\Delta/\Delta}$ was analyzed by confocal microscopy (Fig. 6A). Compared to wild-type the deletion mutant STAT3-ΔNT-CY exhibits a more uniform distribution in non-stimulated cells. Most interestingly, STAT3-ΔNT-CY does not accumulate in the nucleus upon IL-6 stimulation although this mutant becomes tyrosine phosphorylated (Fig. 4B), forms dimers upon phosphorylation (Fig. 4C), and binds to DNA (Fig 6B). Lack of nuclear accumulation of STAT3-ΔNT-CY in response to stimulation has also been observed in transiently transfected $MEF^{\Delta/\Delta}$ and HEK293 cells as well as for non tagged STAT3-ΔNT in transiently transfected $MEF^{\Delta/\Delta}$ (data not shown). With respect to subcellular distribution in unstimulated cells and nuclear accumulation upon stimulation STAT3-VL-CY resembles STAT3-CY.

Nucleocytoplasmic shuttling of STAT3-CY, STAT3-ΔNT-CY, STAT3-VL-CY and CFP-YFP as a control in $MEF^{\Delta/\Delta}$ was analyzed by iFLAP-imaging as previously described (Herrmann et al., 2007). In this assay the equal signals of CFP and YFP in the double-labelled constructs are transformed to zero by a simple algorithm as exemplified for STAT3-CY in the upper part of Fig. 6C. As a consequence of this algorithm bleaching of YFP leads to the generation of a signal. The fate of the signal representing YFP-bleached molecules can be

followed over time throughout the cell. Neighbouring non-bleached cells serve as controls. The YFP-bleached population of STAT3-CY rapidly diffuses through the cytoplasm, the nuclear and the plasma membranes being barriers for free diffusion. However, over time a signal is detectable within the nucleus indicating that a fraction of molecules passed the nuclear membrane. STAT3-VL-CY behaves similar to STAT3-CY (Fig. 6C, second panel). Compared to the two previous constructs cytoplasmic bleaching of STAT3-ΔNT-CY resulted in a stronger nuclear signal after 20 minutes (Fig. 6C, third panel). The diffusion of the bleached CFP-YFP control is also hindered by the nuclear envelope. However, this construct showed the most pronounced nuclear presence after 20 minutes (Fig. 6C, last panel).

10 measurements as depicted in Fig. 6C were performed for each of the four constructs. For quantitative evaluation of the data a cytoplasmic and a nuclear ROI were positioned. The diagrams in Fig. 7 show the averaged normalized cytoplasmic and nuclear fluorescence in these ROIs for each construct. The decay of nuclear YFP fluorescence upon cytoplasmic bleaching of YFP is indicative for nucleocytoplasmic shuttling. The decrease in nuclear YFP fluorescence of STAT3-ΔNT-CY (Fig. 7C) is steeper than in case of the other two STAT3 constructs indicating that STAT3-ΔNT-CY shuttles more rapidly than STAT3-CY (Fig. 7A) and STAT3-VL-CY (Fig. 7B). As has been evident from the selected images in Fig. 6C the CFP-YFP control (Fig. 7D) shuttles even faster than STAT3-ΔNT-CY.

Discussion

While nucleocytoplasmic shuttling of latent STAT3 and nuclear accumulation of activated, i.e. tyrosine phosphorylated STAT3 are well established the molecular mechanisms driving these processes are ill-defined. The subcellular distribution of latent STAT3 with high cytoplasmic and low nuclear concentrations represents a steady state resulting from continuous nuclear import and export (Pranada et al., 2004). Treatment of cells with leptomycin B, an inhibitor of CRM1 (= exportin-1), leads to a partial nuclear accumulation of STAT3 indicating that latent nuclear export is in part dependent on CRM1 (Bhattacharya and Schindler, 2003 and data not shown).

To assess the role of CRM1-dependent nuclear export sequences for nucleocytoplasmic shuttling of latent STAT3 we mutated a putative NES sequence ($QL_{525}TTL_{528}AEKLL$) previously identified to be important for nuclear export of latent STAT3 (Bhattacharya and Schindler, 2003). As previously described the resulting L525A/L528A mutant is enriched in the nuclei of resting cells and accumulates in the nucleus upon stimulation. Unexpectedly, the L525A/L528A mutant shuttles faster between cytoplasm and the nucleus arguing against an impairment of CRM1-mediated export by this mutation. The increased shuttling rate suggests that the nuclear accumulation of this mutant is caused by enhanced nuclear import rather than perturbed export.

The recently solved structure of CRM1 in complex with the export substrate snurportin1 and ranGTP shows that the hydrophobic residues of an NES must be exposed for binding to a hydrophobic pocket of CRM1 (Monecke et al., 2009). Using the structure of the core fragment of STAT3 as a template (Ren et al., 2008) we found that the amino acids L525 and L528 are located on the back of an α-helix in the linker domain of STAT3 (Suppl. Fig. S1). Thus, these residues are buried and the mutations probably have an impact on the integrity of

the domain instead of targeting a functional NES. The same is true for other putative NES sequences identified in the DNA-binding domain and the coiled-coil domain of STAT3 (see Suppl. Fig. S2 and S3). Therefore, the effect of leptomycin B on subcellular distribution of STAT3 might not be mediated by acting on STAT3 directly but possibly on another protein involved in CRM1-mediated export of STAT3. Another possibility is that the NES of STAT3 that interacts with CRM1 has not been identified yet.

Unfortunately, the role of NLS for the nuclear import of activated STAT3 is far from clear. A recent study on STAT1 suggests that a phosphorylated STAT1 dimer interacts in a nonconventional manner with importin α5 without the involvement of a classical NLS (Nardozzi et al., 2010). Several putative NLS within STAT3 have been defined by mutagenesis studies (R214/R215 and R414/417 by Ma et al. (Ma et al., 2003) and aa150-163 by Liu et al. (Liu et al., 2005). However, in some of these studies an impact of the mutation on the integrity of the STAT3 protein cannot be excluded. One of these putative NLS comprising R214 and R215 of STAT3 has been shown to be essential for interaction of STAT3 with importin α5 and nuclear accumulation in response to tyrosine phosphorylation (Ma and Cao, 2006). In another report the R214A/R215A mutant was described to show increased CRM1 dependent nuclear export and a rim-like nuclear staining pattern (Sato et al., 2005). However, our data do not support these observations. R214 and R215 are part of a long α-helix within the coiled-coil domain of STAT3 one being exposed the other being buried (Suppl. Fig. S4). Mutation of these residues in the context of STAT3-CY did not change the subcellular distribution of STAT3 in resting cells but as reported previously impairs nuclear accumulation upon activation. The rate of nucleocytoplasmic shuttling is not affected by the mutation of R214 and R215. From this finding we conclude that nucleocytoplasmic shuttling of latent STAT3 is independent of binding to importin. Possibly nuclear import of latent STAT3 is facilitated by the direct interaction of STAT3 with constituents of the nuclear pore complex as has been reported for STAT1 (Marg et al., 2004).

In the second part of our work we elucidated the importance of dimerization of latent STAT3 for nucleocytoplasmic shuttling. The dimer interface of latent STAT3 has not been identified yet. From recent advances in the understanding of the dimerization of latent STAT1 (Mao et al., 2005) and the crystal structure of the STAT3 core fragment (Ren et al., 2008) we concluded that the N-terminal domain might be important for dimerization of latent STAT3. Indeed, deletion of the N-terminal domain of STAT3 abrogated dimer formation as shown by bnPAGE and 2f-FCS. Point mutations analogous to those that disturb homotypic interaction of the N-terminal domain of STAT1 had no detrimental effect on the dimerization of STAT3. It has recently been shown that the homotypic interaction of the N-terminal domains of STAT1 and STAT3 are of high and low affinity, respectively (Wenta et al., 2008). Therefore, the N-terminal domain of STAT3 might not contribute to STAT3 dimerization by homotypic interaction but by reciprocal interactions with another domain of STAT3. The SH2-domain could be a candidate for an interaction with the N-terminal domain because it has been shown, that mutation of the SH2-domain affects dimer formation of unphosphorylated STAT3 (Kretzschmar et al., 2003). Such an interaction would lead to an antiparallel orientation of the latent STAT3 dimer in contrast to the parallel orientation of the activated STAT3 dimer (Becker et al., 1998). The fact that monomeric latent STAT3-ΔNT shuttles between the nucleus and the cytoplasm indicates that dimerization of latent STAT3 is not required for nucleocytoplasmic shuttling. STAT3-ΔNT shuttles faster than wildtype suggesting that dimerization might even hinder nucleocytoplasmic shuttling of latent STAT3.

STAT3 lacking the N-terminal domain becomes phosphorylated and dimerizes in response to IL-6 stimulation. Thus, latent dimerization is not required for activation of STAT3 at the receptor. Furthermore, the N-terminal domain is not essential for the dimerization of phosphorylated STAT3. Activated STAT3 that lacks the N-terminal domain binds to DNA ((Zhang and Darnell, 2001) and Fig. 6B). From the crystal structure of the phosphorylated STAT3 core fragment (lacking the N-terminal domain) bound to DNA it is evident that

dimerization is mainly driven by phosphotyrosine-SH2 domain interactions and stabilized by DNA-binding (Becker et al., 1998). The result that phosphorylated STAT3 dimers lacking the N-terminal domain do not accumulate in the nucleus was unexpected (Zhang et al., 2006). However, a similar contribution of the N-terminal domain for nuclear accumulation has been shown for STAT1 (Meissner et al., 2004). This finding points to an unprecedented role of the N-terminal domain for nuclear import of activated STAT3 that deserves further investigation.

Materials and Methods hier noch den EMSA einfügen

Recombinant plasmids

The expression vector pSVL-STAT3-CY described previously (Pranada et al., 2004) served as a basis for cloning pcDNA5/FRT/TO-STAT3-CY using the pcDNA5/FRT/TO vector of the Flp-In system (Invitrogen, USA). pcDNA5/FRT/TO-STAT3-CY was used as template for cloning the constructs STAT3-ΔNLS-CY, STAT3-ΔNES-CY, STAT3-VL-CY and STAT3-ΔNT-CY.

The STAT3 point mutants were generated by PCR with the following primers: R214A/R215A sense (5'-cagatggcgg caagcattg-3'), antisense (5'-caatgcttgc cgccatctg-3'); L525A/L528A sense (5'-aggcgacaac ggcggctgag aagc-3'), antisense (5'-cagccgccgt tgtcgcctgc tcg-3'); V77A/L78A sense (5'-gagtccaatg ccgcctatca gcac-3'), antisense (5'-gtgctgatag gcggcattgg actc-3'). The deletion mutant ΔNT encoding amino acids 126-770 of STAT3 was generated by PCR introducing a XhoI site and a start codon with the sense primer (5'-tattctcgag atgcagcaag ggggccaggc caa-3'). The products were analyzed and cloned into pcDNA5/FRT/TO-STAT3-CY. For cloning of CFP-YFP, STAT3-CY was used as a template and a XhoI site and a start codon was introduced by PCR with the sense primer (5'-atccgctcga gcgctaccgg tcgccac-3'). The product was sequenced and transferred into pcDNA5/FRT/TO. The eGFP labelled constructs were generated by replacing the CY-tag with eGFP. eGFP was expressed using the peGFP-N1 vector (Invitrogen).

Cytokines and cytokine receptors

Recombinant human IL-6 was expressed in *Escherichia coli*, refolded, and purified as described previously (Arcone et al., 1991). The specific activity of IL-6 was measured by a B9 cell proliferation assay. sIL-6Rα was expressed in insect cells as previously described (Weiergräber et al., 1995).

Cell culture and transfection

Murine embryonal fibroblast $MEF^{fl/fl}$ and $MEF^{\Delta/\Delta}$ (generous gift of Prof. V. Poli, Torino, Italy) were grown in Dulbecco's Modified Eagle Medium (DMEM) with GlutaMax™ (Invitrogen, USA) supplemented with 10% FCS, 100 U/ml penicillin and 100 µg/ml streptomycin (BIO-Whittaker, Verviers, Belgium). COS-7 cells were cultivated in phenol red free DMEM with 10% FCS. The cells were incubated at 37°C in a water-saturated atmosphere at 5% CO_2. $MEF^{\Delta/\Delta}$ cells were stably reconstituted with STAT3-CY, STAT3-ΔNLS-CY, STAT3-ΔNES-CY, STAT-VL-CY, STAT3-ΔNT-CY or CFP-YFP using the Flp-In system (Invitrogen, USA) ensuring integration of the different constructs at the same locus.

Preparation of cell lysates, SDS-PAGE and immunoblotting

MEF cells were cultured on 6-well plates. The cells were stimulated with 20 ng/ml IL-6 and 500 ng/ml sIL-6Rα for 30 minutes or left untreated. Subsequently, cells were lysed with RIPA lysis buffer (50 mM Tris-HCl, pH 7.4, 150 mM NaCl, 1 mM EDTA, 0.5% Nonidet P-40, 1 mM NaF, 15% glycerol, 20mM β-glycerophosphate, 1 mM Na_3VO_4, 0.25 mM phenylmethylsulfonylfluoride, 5 g/ml aprotinin, and 1 g/ml leupeptin). The lysates were analyzed with SDS-PAGE, Western blotting and immunodetection using antibodies directed against phosphotyrosine^{705}-STAT3 (Cell Signaling Technology, MA, USA), STAT3 (H190, Santa Cruz Biotechnology, CA, USA), GAPDH (Santa Cruz, CA, USA) and HRP conjugated secondary antibodies (Dako, Hamburg, Germany). All antibodies were used in a 1:1.000 dilution in TBS-N (20 mM Tris-HCl, pH 7.6, 137 mM NaCl and 0.1% Nonidet P-40) and detected by chemiluminescence (ECL, Millipore, MA, USA).

Blue-native PAGE and detection of CFP and YFP

MEF cells were cultured on 10 cm dishes. The cells were stimulated with 25 ng/ml IL-6 and 500 ng/ml sIL-6Rα for 30 minutes or left untreated. The cells were lysed in Brij-96V lysis

buffer (0.1 M phosphate buffer pH 8.0, 0.5% Brij-96V, 1.5% glycerol, 0.5 mM EDTA,1 mM Na_3VO_4, 0.25 mM phenylmethylsulfonylfluoride, 5 g/ml aprotinin, and 1 g/ml leupeptin). The lysates were incubated with Coomassie Brilliant Blue G-250 (Serva, Heidelberg, Germany) to a final concentration of 0.2% and separated by blue-native PAGE (Schägger et al., 1994) using a gradient polyacrylamide gel (4 to 20%). The cathode buffer was composed of 50 mM Tricine, 15 mM Bistris and 0.02% Coomassie Brilliant Blue G-250, the anode buffer contained 50 mM Bistris/HCl pH 7. The YFP-fluorescence was analyzed with a Typhoon gel fluorescence scanner (Amersham Biosciences) by excitation with a 488 nm laser line. The emission was detected using a 515-555 nm bandpass filter.

Preparation of nuclear extracts and electrophoretic mobility shift assay (EMSA)

After stimulation the MEF were washed two times and harvested with PBS containing sodium vanadate. The pellet was resuspended in buffer A (10 mM HEPES/KOH pH 7.9, 1.5 mM $MgCl_2$, 10 mM KCl, 0.5 mM DTT, 0.2 mM PMSF, 1 mM sodium vanadate), sonified for 10 sec, incubated 10 minutes on ice and centrifuged 10 sec at 13,000 rpm. The pellet was resuspended in buffer C (20 mM Hepes/KOH pH 7.9, 420 mM NaCl, 1.5 mM $MgCl_2$, 0.2 mM EDTA, 25% glycerol, 0.5 mM DTT, 0.2 mM PMSF, 1 mM sodium vanadate), incubated 20 minutes on ice and centrifuged 2 minutes at 13,000 rpm. Protein concentrations of the supernatants were measured with the Bio-Rad protein assay (Bio-Rad, Richmond, USA). A double-stranded mutated *sis*-inducible element (SIE) oligonuleotide from the *c-fos* promotor (m67SIE: 5´-GAT CCG GGA GGG ATT TAC GGG AAA TGC TG-3´) was labeled by filling in 5´-protruding ends with the Klenow enzyme using [α-^{32}P]dATP. Nuclear extracts containing 3,5 µg protein were incubated with about 10 fmol (10,000 cpm) of labelled oligonucleotides in gel shift incubation buffer (10 mM HEPES (pH 7.8), 1 mM EDTA, 5 mM $MgCl_2$, 10% glycerol, 5 mM DTT, 2 mM PMSF, 0.05 mg/ml of poly(dI-dC), and 1 mg/ml BSA) for 10 minutes at room temperature. The DNA/protein complexes were separated on a

4.5% polyacrylamide gel containing 7.5% glycerol in 0.25% TBE (200 mM Tris, 166 mM boric acid, 2 mM EDTA, adjusted to pH 8.3) at 20 V/cm. Gels were fixed in 10% methanol and 10% acetic acid for 15 minutes, dried and analyzed by autoradiography.

Indirect immunofluorescence

MEF cells were grown on glass coverslips, washed twice with phosphate-buffered saline (PBS) containing 1 mM $MgCl_2$ and 0.1 mM $CaCl_2$ (PBS^{++}) and fixed with -20°C cold methanol for 15 minutes. Subsequently, the cells were permeabilized with PBS^{++} containing 0.1% Triton X-100 ($PBST^{++}$) for 5 minutes, quenched with 50 mM NH_4Cl in $PBST^{++}$ and blocked with $PBST^{++}$ containing 1% BSA (SERVA, Heidelberg, Germany). Immunostaining was performed using a STAT3 antibody (124H6, Cell Signaling, USA) and a secondary antibody conjugated with Cy2 (Jackson Immunolaboratories, PA, USA). The antibodies were diluted 1:200 in $PBST^{++}$ containing 0.2% BSA. The cells were incubated for 60 minutes with the specific STAT3 antibody, washed twice with $PBST^{++}$ and incubated with the secondary antibody for 60 minutes. The coverslips were dipped in water and mounted with ImmuMount (Shandon, PA, USA).

Confocal fluorescence microscopy and live cell imaging

The confocal imaging was performed with a Zeiss LSM 510Meta confocal microscope (Zeiss, Jena, Germany). CFP and YFP fluorescence were detected as described previously (Pranada et al., 2004). Cy2 fluorescence was detected using the 488 nm line of the argon laser, a 488 nm dichroic mirror and a 505-530 nm bandpass filter. The images shown represent confocal slices of approximately 1 µm. The cells were examined with a 63x 1.2 NA Zeiss water immersion objective. For fixation stably transfected $MEF^{\Delta/\Delta}$ cells were grown on glass coverslips for 48 h. The cells were fixed with 3.7% paraformaldehyde for 15 minutes and washed twice with PBS^{++}. Subsequently the cells were quenched with 50 mM NH_4Cl in PBS^{++} for 5 minutes, dipped in water and mounted with ImmuMount.

For live cell imaging stably transfected $MEF^{\Delta/\Delta}$ cells were grown on 42 mm glass coverslips. After 48 hours the coverslips were placed into a thermostatted (37°C) and CO_2-controlled incubation chamber (Pecon, Erbach, Germany) and flushed with phenol red free DMEM (Invitrogen, USA). iFLAP experiments were performed as described previously (Pranada et al., 2004). To analyze the shuttling by calculating the ratio of CFP and YFP fluorescence the iFLAP method was modified (Herrmann et al., 2007). The CFP and YFP signals from STAT3-CY were adjusted to equal intensities. A signal was generated by bleaching the YFP moiety in a cytoplasmic ROI with the 514 nm line of the argon laser during data recording. Depicted intensities were calculated using the algorithm (1 – iYFP/iCFP) x 4096 = $iYFP_{bleach}$ (12bit picture).

Dual-focus fluorescence correlations spectroscopy (2f-FCS)

COS-7 cells were transfected with 2 µg of plasmids encoding eGFP, STAT3-eGFP and STAT3-ΔNT-eGFP using Mirus TransIT-LT1 transfection reagent (Mirus Bio Corp., Madison, USA). The cells were lysed in Brij-96V lysis buffer (composed as described above but lacking glycerol).

The 2f-FCS experiments were carried out using a setup based on a standard confocal epi-fluorescence microscope (Böhmer et al., 2001). eGFP and eGFP tagged fusion constructs were excited with a 470 nm laser beam (LDH-P-C-470B). The fluorescent emission light was split from the excitation light by using a clearup bandpass filter (490-520 nm). The light is focused by confocal optics with a pinhole diameter of 200 µm onto a single photon avalanche diode (SPAD, PDM series, Micro Photon Devices, Bolzano, Italy). The temperature was controlled, using a home-made thermostatted device at 25°C (Müller and Richtering, 2008).

An adequate model (Dertinger et al., 2007) for ACF/CCF is given by:

$$g(t,\delta,\mathbf{v}) = \frac{c}{4}\sqrt{\frac{\pi}{Dt}}\int dz_1 \int dz_2 \frac{\kappa(z_1)\kappa(z_2)}{8Dt + w^2(z_1) + w^2(z_2)} \times \exp\left[-\frac{(z_2 - z_1 - v_z t)^2}{4Dt} - 2\frac{(\delta - v_x t)^2 + v_y^2 t^2}{8Dt + w^2(z_1) + w^2(z_2)}\right]$$

where δ is the lateral distance between the detection volume centers, ε_1 and ε_2 are factors proportional to overall excitation intensity and detection efficiency in each laser, c is the concentration of the fluorescent molecules and D is the diffusion coefficient. The functions of κ(z) and w(z) are given by the following equations:

$$w(z) = w_0\left[1 + \left(\frac{\lambda_{ex} z}{\pi w_0^2 n}\right)^2\right]^{1/2}$$

and

$$\kappa(z) = 2\int_0^a \frac{d\rho\rho}{R^2(z)} \exp\left(-\frac{2\rho^2}{R^2(z)}\right) = 1 - \exp\left(-\frac{2a^2}{R^2(z)}\right)$$

with

$$R(z) = R_0\left[1 + \left(\frac{\lambda_{em} z}{\pi R_0^2 n}\right)^2\right]^{1/2}$$

where λ_{ex} and λ_{em} are excitation and emission wavelengths, n is the refractive index of the sample, α is the confocal pinhole radius, and ω_0 and R_0 are fit parameters (Müller et al., 2008).

2f-FCS experiments were performed with three independent samples per construct and over 120 minutes detection time for each measurement point.

The fitting procedure of experimental data is carried out globally for both the ACFs and CCF using single particle diffusion model including triplet state correction (without necessity to imply a dual particle diffusion model suggesting a second slow-moving component).

Molecular mass estimation of the measured particles (assuming spherical symmetry) was calculated with the known molecular mass of eGFP (27 kDa) using the following equation:

$$MM_{sample} = \left(\frac{D_{eGFP}}{D_{sample}}\right)^3 \times MM_{eGFP}$$

where MM is the molecular mass, and D is the diffusion coefficient from 2f-FCS experiments.

Acknowledgements

The project was supported by the Deutsche Forschungsgemeinschaft (SFB 542 projects B12 and Z1), the European Community (Marie Curie Research and Training Network ReceptEUR) and the excellence initiative of the German federal and state governments.

.

References

Arcone, R., Pucci, P., Zappacosta, F., Fontaine, V., Malorni, A., Marino, G. and Ciliberto, G. (1991). Single-step purification and structural characterization of human interleukin-6 produced in Escherichia coli from a T7 RNA polymerase expression vector. *Eur J Biochem* **198**, 541-547.

Becker, S., Groner, B. and Müller, C. W. (1998). Three-dimensional structure of the Stat3b homodimer bound to DNA. *Nature* **394**, 145-151.

Bhattacharya, S. and Schindler, C. (2003). Regulation of Stat3 nuclear export. *J Clin Invest* **111**, 553-559.

Böhmer, M., Pampaloni, F., Wahl, M., Rahn, H. J., Erdmann, R. and Enderlein, J. (2001). Advanced Time-Resolved Confocal Scanning Device For Ultrasensitive Fluorescence Detection,. *Rev. Sci. Instrum.* **72**, 4145-52.

Braunstein, J., Brutsaert, S., Olson, R. and Schindler, C. (2003). STATs dimerize in the absence of phosphorylation. *J Biol Chem* **278**, 34133-40.

Dertinger, T., Pacheco, V., von der Hocht, I., Hartmann, R., Gregor, I. and Enderlein, J. (2007). Two-focus fluorescence correlation spectroscopy: a new tool for accurate and absolute diffusion measurements. *Chemphyschem* **8**, 433-43.

Frahm, T., Hauser, H. and Koster, M. (2006). IFN-type-I-mediated signaling is regulated by modulation of STAT2 nuclear export. *J Cell Sci* **119**, 1092-104.

Haan, S., Kortylewski, M., Behrmann, I., Muller-Esterl, W., Heinrich, P. C. and Schaper, F. (2000). Cytoplasmic STAT proteins associate prior to activation. *Biochem J* **345**, 417-21.

Herrmann, A., Vogt, M., Monnigmann, M., Clahsen, T., Sommer, U., Haan, S., Poli, V., Heinrich, P. C. and Müller-Newen, G. (2007). Nucleocytoplasmic shuttling of persistently activated STAT3. *J Cell Sci* **120**, 3249-61.

Kim, S. A. and Schwille, P. (2003). Intracellular applications of fluorescence correlation spectroscopy: prospects for neuroscience. *Curr Opin Neurobiol* **13**, 583-90.

Kretzschmar, A. K., Dinger, M. C., Henze, C., Brocke-Heidrich, K. and Horn, F. (2003). Analysis of Stat3 dimerization by fluorescence resonance energy transfer in living cells. *Biochem J* **Pt**.

Levy, D. E. and Darnell, J. E., Jr. (2002). Stats: transcriptional control and biological impact. *Nat Rev Mol Cell Biol* **3**, 651-62.

Levy, D. E. and Lee, C. K. (2002). What does Stat3 do? *J Clin Invest* **109**, 1143-1148.

Liu, L., McBride, K. M. and Reich, N. C. (2005). STAT3 nuclear import is independent of tyrosine phosphorylation and mediated by importin-alpha3. *Proc Natl Acad Sci U S A* **102**, 8150-5.

Ma, J. and Cao, X. (2006). Regulation of Stat3 nuclear import by importin alpha5 and importin alpha7 via two different functional sequence elements. *Cell Signal* **18**, 1117-1126.

Ma, J., Zhang, T., Novotny-Diermayr, V., Tan, A. L. and Cao, X. (2003). A novel sequence in the coiled-coil domain of Stat3 essential for its nuclear translocation. *J Biol Chem* **278**, 29252-60.

Mao, X., Ren, Z., Parker, G. N., Sondermann, H., Pastorello, M. A., Wang, W., McMurray, J. S., Demeler, B., Darnell, J. E., Jr. and Chen, X. (2005). Structural bases of unphosphorylated STAT1 association and receptor binding. *Mol Cell* **17**, 761-71.

Marg, A., Shan, Y., Meyer, T., Meissner, T., Brandenburg, M. and Vinkemeier, U. (2004). Nucleocytoplasmic shuttling by nucleoporins Nup153 and Nup214 and CRM1-dependent nuclear export control the subcellular distribution of latent Stat1. *J Cell Biol* **165**, 823-833.

Meissner, T., Krause, E., Lodige, I. and Vinkemeier, U. (2004). Arginine methylation of STAT1: a reassessment. *Cell* **119**, 587-9; discussion 589-590.

Meyer, T. and Vinkemeier, U. (2004). Nucleocytoplasmic shuttling of STAT transcription factors. *Eur J Biochem* **271**, 4606-12.

Monecke, T., Guttler, T., Neumann, P., Dickmanns, A., Gorlich, D. and Ficner, R. (2009). Crystal structure of the nuclear export receptor CRM1 in complex with Snurportin1 and RanGTP. *Science* **324**, 1087-91.

Müller, C. B., Loman, A., Pacheco, V., Koberling, F., Willibold, D., Richtering, W. and Enderlein, J. (2008). Precise measurement of diffusion by multi-color dual-focus fluorescence correlation spectroscopy. *Eur. Phys. Lett.* **83**, 1-5.

Müller, C. B. and Richtering, W. (2008). Sealed and temperature-controlled sample cell for inverted and confocal microscopes and correlation spectroscopy. *Colloid Polym. Sci.* **286**, 1215-1222.

Nardozzi, J., Wenta, N., Yasuhara, N., Vinkemeier, U. and Cingolani, G. (2010). Molecular basis for the recognition of phosphorylated STAT1 by importin alpha5. *J Mol Biol* **402**, 83-100.

Pranada, A. L., Metz, S., Herrmann, A., Heinrich, P. C. and Müller-Newen, G. (2004). Real time analysis of STAT3 nucleocytoplasmic shuttling. *J Biol Chem* **279**, 15114-15123.

Ren, Z., Mao, X., Mertens, C., Krishnaraj, R., Qin, J., Mandal, P. K., Romanowski, M. J., McMurray, J. S. and Chen, X. (2008). Crystal structure of unphosphorylated STAT3 core fragment. *Biochem Biophys Res Commun* **374**, 1-5.

Sato, N., Tsuruma, R., Imoto, S., Sekine, Y., Muromoto, R., Sugiyama, K. and Matsuda, T. (2005). Nuclear retention of STAT3 through the coiled-coil domain regulates its activity. *Biochem Biophys Res Commun* **336**, 617-24.

Schägger, H., Cramer, W. A. and von Jagow, G. (1994). Analysis of molecular masses and oligomeric states of protein complexes by blue native electrophoresis and isolation of membrane protein complexes by two-dimensional native electrophoresis. *Anal Biochem* **217**, 220-30.

Weiergräber, O., Hemmann, U., Küster, A., Müller-Newen, G., Schneider, J., Rose-John, S., Kurschat, P., Brakenhoff, J. P., Hart, M. H., Stabel, S. et al. (1995). Soluble human interleukin-6 receptor: expression in insect cells, purification and characterization. *Eur J Biochem* **234**, 661-669.

Wenta, N., Strauss, H., Meyer, S. and Vinkemeier, U. (2008). Tyrosine phosphorylation regulates the partitioning of STAT1 between different dimer conformations. *Proc Natl Acad Sci U S A* **105**, 9238-43.

Yu, H. and Jove, R. (2004). The STATs of cancer - new molecular targets come of age. *Nat Rev Cancer* **4**, 97-105.

Zhang, L., Badgwell, D. B., Bevers, J. J., 3rd, Schlessinger, K., Murray, P. J., Levy, D. E. and Watowich, S. S. (2006). IL-6 signaling via the STAT3/SOCS3 pathway: functional analysis of the conserved STAT3 N-domain. *Mol Cell Biochem* **288**, 179-89.

Zhang, X. and Darnell, J. E., Jr. (2001). Functional importance of Stat3 tetramerization in activation of the alpha 2-macroglobulin gene. *J Biol Chem* **276**, 33576-81.

Legends to Figures

Figure 1: Analysis of nucleocytoplasmic shuttling using STAT3-CY.

(A) Selective bleaching of YFP in STAT3-CY. $MEF^{\Delta/\Delta}$ stably transfected with STAT3-CY were fixed and images of a single cell were taken using the YFP and the CFP channels of a confocal microscope. A pattern was bleached representing the lettering and icon of the *Collaborative Research Center SFB 542* using the 514 nm laser of the confocal microscope. Subsequently, images were taken under the same conditions as before bleaching. The bleached pattern is only visible in the YFP channel. The CFP fluorescence is unaffected by the bleaching procedure. Scale bars represent 10 µm.

(B) Set-up of the shuttling assay. Nucleocytoplasmic shuttling was analyzed in single living $MEF^{\Delta/\Delta}$ cells stably transfected with STAT3-CY constructs. For this purpose the YFP moiety of STAT3-CY was irreversibly bleached in a cytoplasmic region of interest (ROI, white circle). CFP and YFP fluorescence was monitored in a cytoplasmic ROI, a nuclear ROI and an extracellular ROI for the detection of background fluorescence (red circles). The CFP and YFP fluorescence measured are depicted in the diagrams. The transient increase of CFP fluorescence in the cytoplasmic ROI is a result of the loss of FRET between CFP and YFP upon bleaching of YFP. The CFP signal decreases over time because of redistribution of the bleached molecules within the cytoplasm. Decay of nuclear YFP fluorescence in the presence of a constant CFP signal is indicative for nucleocytoplasmic shuttling of STAT3-CY. Scale bars represent 10 µm.

(C) Subcellular localization of endogenous STAT3 and fluorescently labelled STAT3-CY. $MEF^{fl/fl}$, $MEF^{\Delta/\Delta}$ and $MEF^{\Delta/\Delta}$ stably transfected with STAT3-CY ($MEF^{\Delta/\Delta}$STAT3-CY) were stimulated with 20 ng/ml IL-6 and 0.5 µg/ml soluble IL-6R (sR) for 30 minutes or left untreated. All cells were fixed. $MEF^{fl/fl}$ and $MEF^{\Delta/\Delta}$ were permeabilized and prepared for immune fluorescence (IF) using a STAT3 antibody followed by incubation with a Cy2-

labelled secondary antibody. Cells were analyzed by confocal microscopy. Scale bars represent 20 µm.

Figure 2: Characterization of STAT3-CY and putative NLS and NES mutants.

(A) Schematic representation of the domain structure of STAT3-CY and mutants used for the generation of stable cell lines. Red bars show the positions of the indicated point mutations. NT, N-terminal domain; CC, coiled-coil domain; DB, DNA-binding domain; SH2, src-homology 2 domain; TA, transactivation domain.

(B) $MEF^{\Delta/\Delta}$ stably transfected with STAT3-CY, STAT3-ΔNLS-CY or STAT3-ΔNES-CY or $MEF^{fl/fl}$ were stimulated with 20 ng/ml IL-6 and 0.5 µg/ml soluble IL-6R (sR) for 30 minutes or left untreated. Cellular lysates were analyzed by immunoblotting using antibodies against phosphotyrosine 705 of STAT3, STAT3 and GAPDH as a loading control.

(C) $MEF^{\Delta/\Delta}$ stably transfected with STAT3-CY, STAT3-ΔNLS-CY or STAT3-ΔNES-CY were stimulated with 20 ng/ml IL-6 and 0.5 µg/ml soluble IL-6R (sR) for 30 minutes or left untreated. Cells were fixed and analyzed by confocal microscopy. Scale bars represent 20 µm.

Figure 3: Nucleocytoplasmic shuttling of (A) STAT3-CY, (B) STAT3-ΔNLS-CY and (C) STAT3-ΔNES-CY in stably transfected $MEF^{\Delta/\Delta}$.

The shuttling assay was performed at a confocal microscope as described in the legend to Fig. 1B. Living cells were analyzed in a incubation chamber at 37°C. The diagrams show the normalized and then averaged cytoplasmic and nuclear YFP fluorescence over time from n experiments as indicated. The bars at the x-axis represent the duration of the cytoplasmic bleach pulses. Only experiments with constant nuclear CFP fluorescence (not shown) were evaluated. (D) In this control experiment the same cells as in (A) were used but the bleach-ROI was located outside of the cell. The constant YFP fluorescence in the cytoplasmic and nuclear ROIs indicate that data recording does not contribute to bleaching of the fluorophore.

Figure 4: Role of the N-terminal domain in dimerization of STAT3.

(A) Schematic representation of the domain structure of STAT3-CY and mutants used for the generation of stable cell lines. The red bar shows the position of the indicated point mutations. NT, N-terminal domain; CC, coiled-coil domain; DB, DNA-binding domain; SH2, src-homology 2 domain; TA, transactivation domain.

(B) $MEF^{\Delta/\Delta}$ stably transfected with STAT3-VL-CY or STAT3-ΔNT-CY were stimulated with 20 ng/ml IL-6 and 0.5 µg/ml soluble IL-6R (sR) for 30 minutes or left untreated. Cellular lysates were analyzed by immunoblotting using antibodies against phosphotyrosine 705 of STAT3, STAT3 and GAPDH as a loading control.

(C) $MEF^{\Delta/\Delta}$ stably transfected with STAT3-CY, STAT3-VL-CY or STAT3-ΔNT-CY or $MEF^{fl/fl}$ were stimulated with 25 ng/ml IL-6 and 0.5 µg/ml soluble IL-6R (sR) for 30 minutes or left untreated. After mild lysis (0.5% Brij-96V) of the cells 30 µg of protein were incubated with Coomassie Brilliant blue G-250 and separated on a native gradient gel (4-20% PAA). The wet gel was analyzed on a fluorescence scanner.

Figure 5: Analysis of STAT3-eGFP and STAT3-ΔNT-eGFP by 2f-FCS.

Auto- and cross-correlation functions (ACF and CCF, respectively) from 2f-FCS experiments on (A) eGFP, (B) STAT3-eGFP and (C) STAT3-ΔNT-eGFP. Experimental data points were fitted (lines) using a single particle diffusion model including triplet state correction.

Figure 6: Confocal analysis of N-terminal STAT3 mutants.

(A) $MEF^{\Delta/\Delta}$ stably transfected with STAT3-CY, STAT3-ΔNT-CY or STAT3-VL-CY were stimulated with 20 ng/ml IL-6 and 0.5 µg/ml soluble IL-6R (sR) for 30 minutes or left untreated. Living cells were analyzed by confocal microscopy. Scale bars represent 20 µm. (B) $MEF^{\Delta/\Delta}$ stably transfected with STAT3-CY, STAT3-ΔNT-CY or STAT3-VL-CY were stimulated with 20 ng/ml IL-6 and 1 µg/ml soluble IL-6R (sR) for 30 minutes or left

untreated. Nuclear extracts were prepared and analyzed in an electrophoretic mobility shift assay (EMSA) using the *sis*-inducible element (SIE) that contains a STAT3 binding site.

(C) Imaging of nucleocytoplasmic shuttling of. STAT3-CY, STAT3-VL-CY, STAT3-ΔNT-CY and CFP-YFP in stably transfected $MEF^{\Delta/\Delta}$. Living cells were analyzed in a incubation chamber at 37°C at a confocal microscope. The YFP and CFP channels of the confocal microscope were adjusted in a way that the YFP and CFP fluorescence of the STAT3-CY constructs appear with the same intensities. For each pixel of the image the intensity of the YFP (iYFP) and CFP fluorescence (iCFP) were used with the equation (1 – iYFP/iCFP) x 4096 = $iYFP_{bleach}$, to calculate a new image that represents only YFP bleached molecules. Intensities are shown in rainbow colors with blue representing weak and red strong signals. White rectangles represent the bleach ROIs used for the generation of YFP bleached STAT3-CY molecules. Scale bars represent 20 µm.

Figure 7: Nucleocytoplasmic shuttling of (A) STAT3-CY, (B) STAT3-VL-CY, (C) STAT3-ΔNT-CY and (D) CFP-YFP in stably transfected $MEF^{\Delta/\Delta}$.

The shuttling assay was performed at a confocal microscope as described in the legend to Fig. 6C. Living cells were analyzed in a incubation chamber at 37°C. The diagrams show the normalized and then averaged YFP fluorescence in cytoplasmic and nuclear ROIs over time from 10 experiments for each construct. Only experiments with constant nuclear CFP fluorescence (not shown) were evaluated.

A fixed cells:

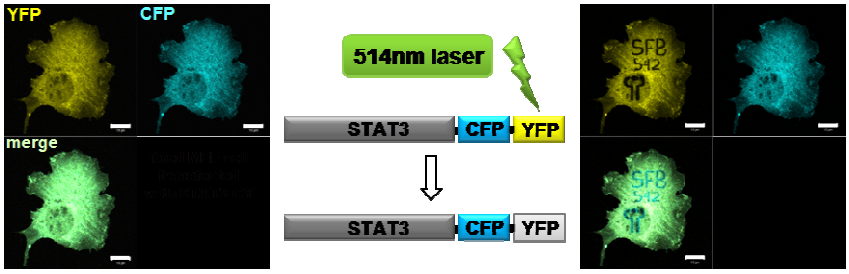

B living cells:

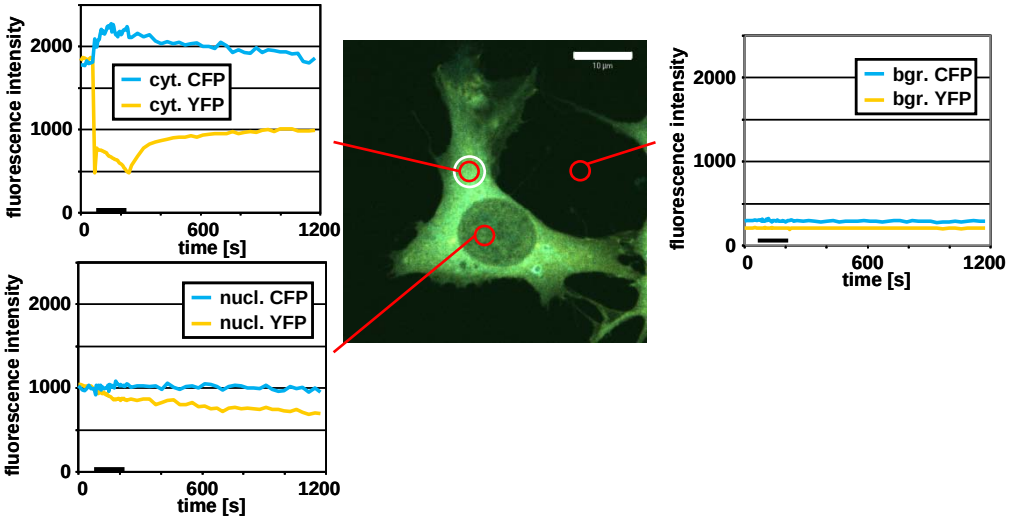

C

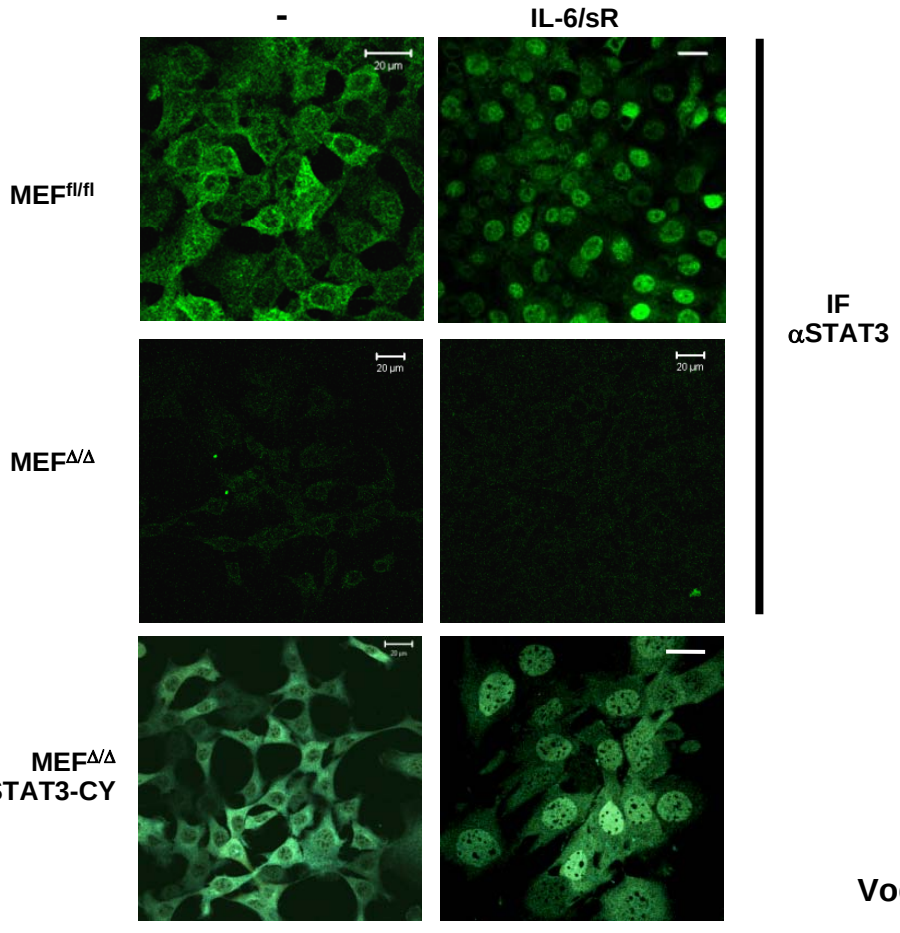

Vogt et al. Fig. 1

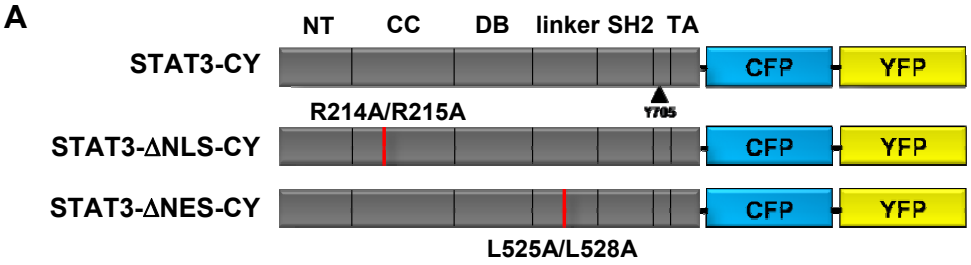

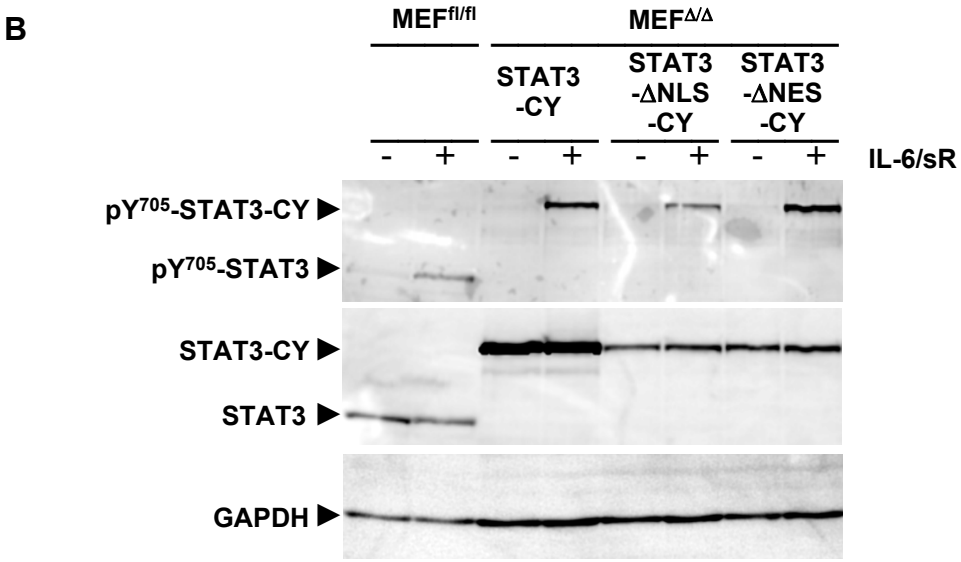

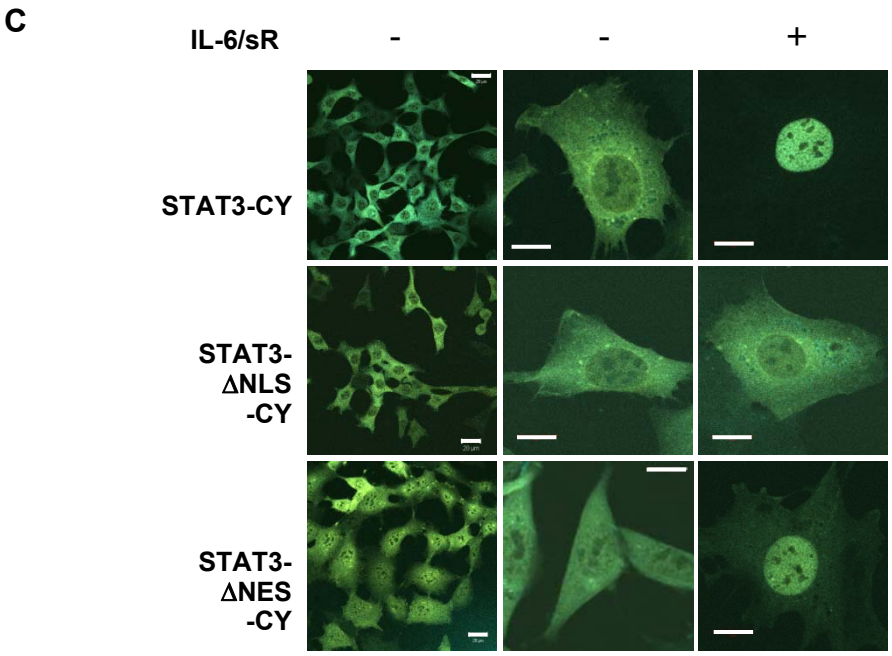

Vogt et al. Fig. 2

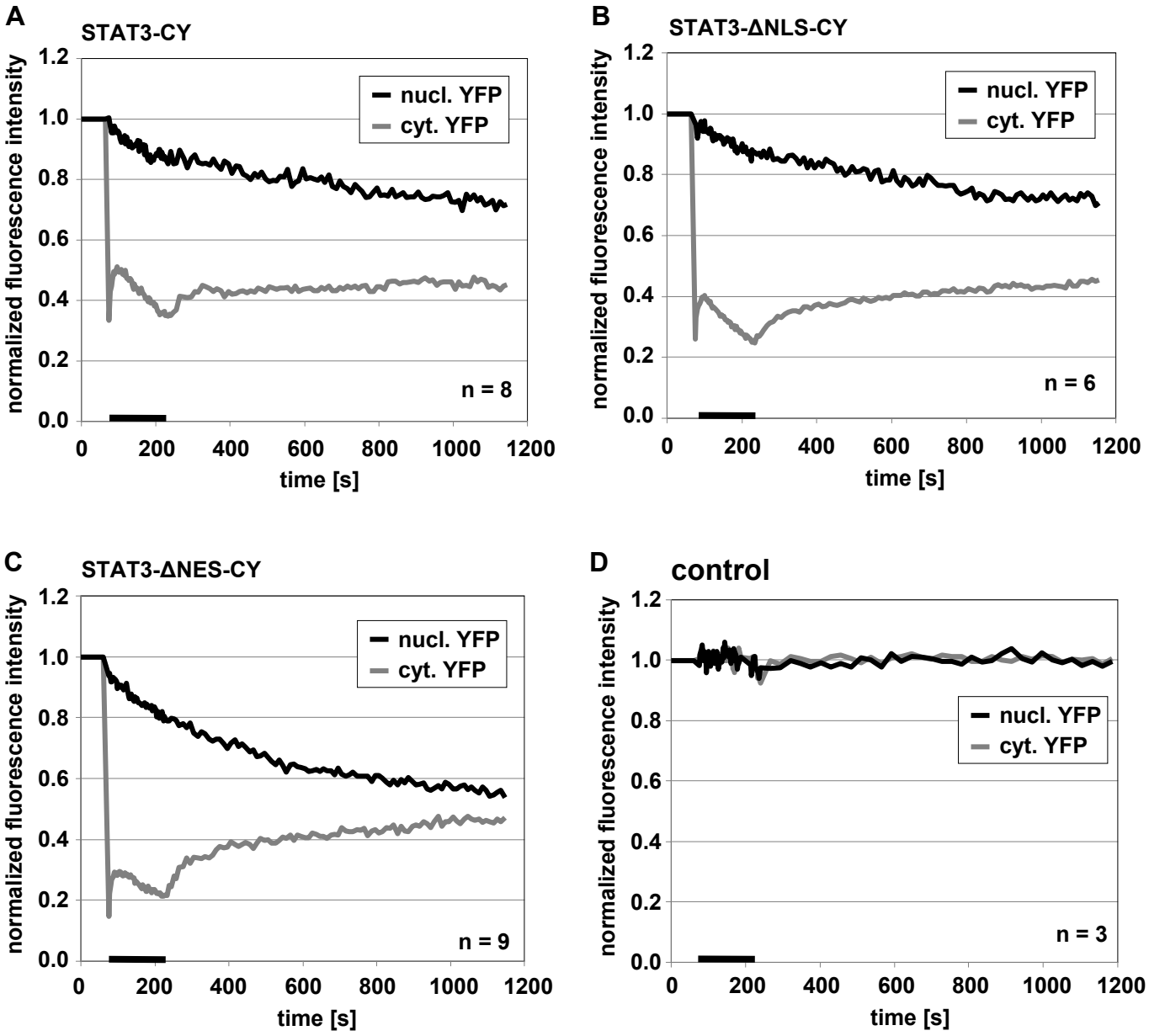

Vogt et al. Fig. 3

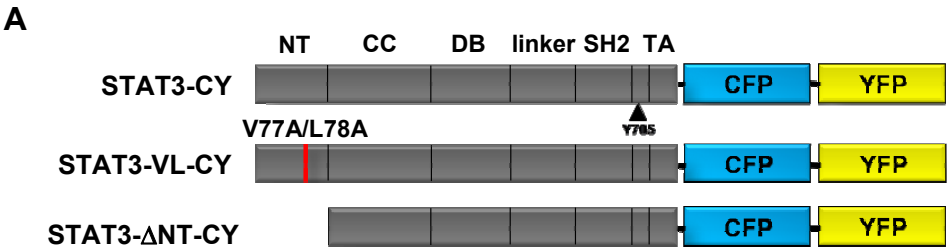

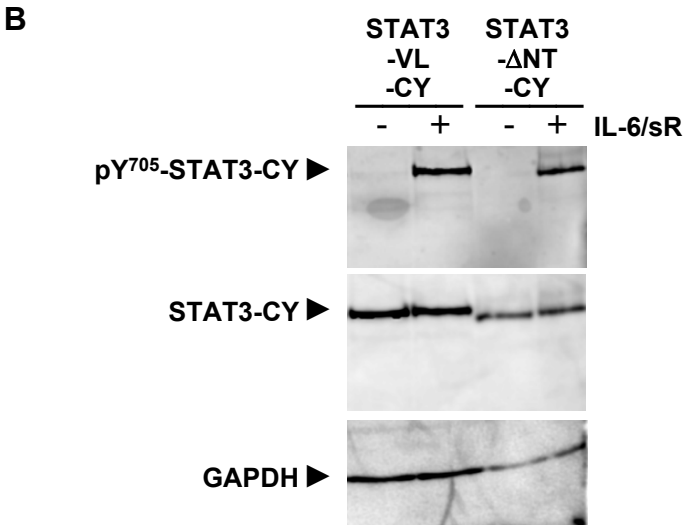

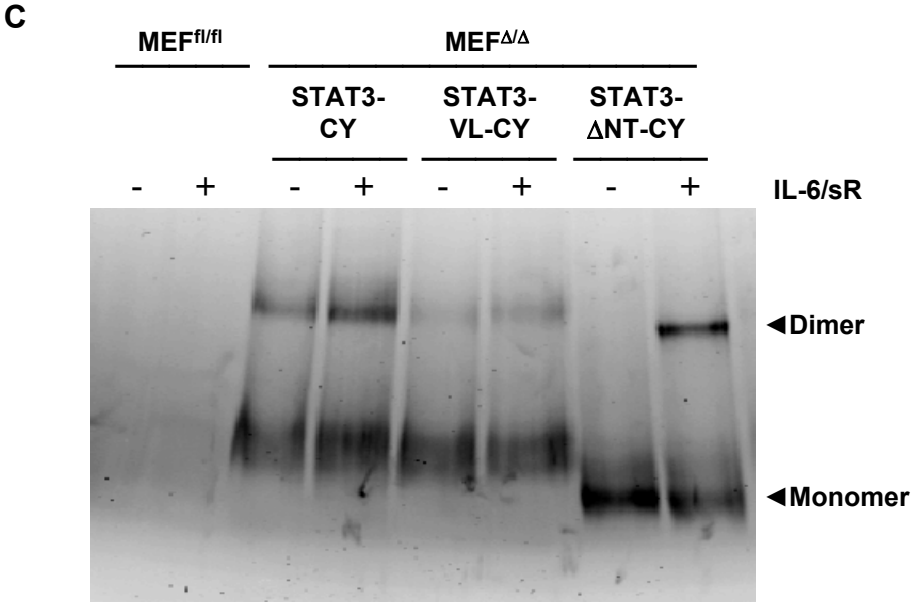

Vogt et al. Fig. 4

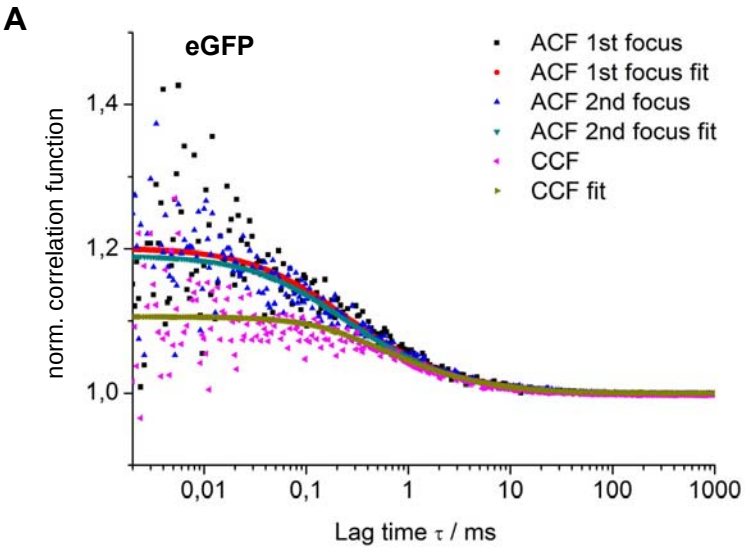

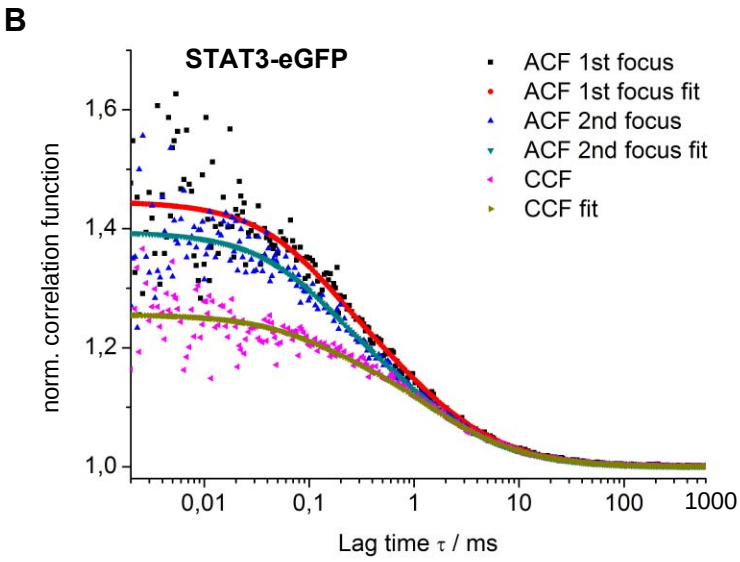

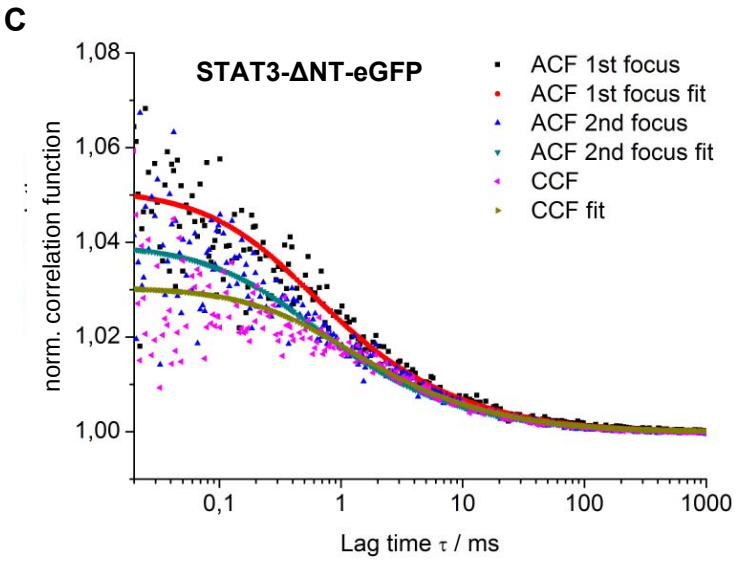

Vogt et al. Fig. 5

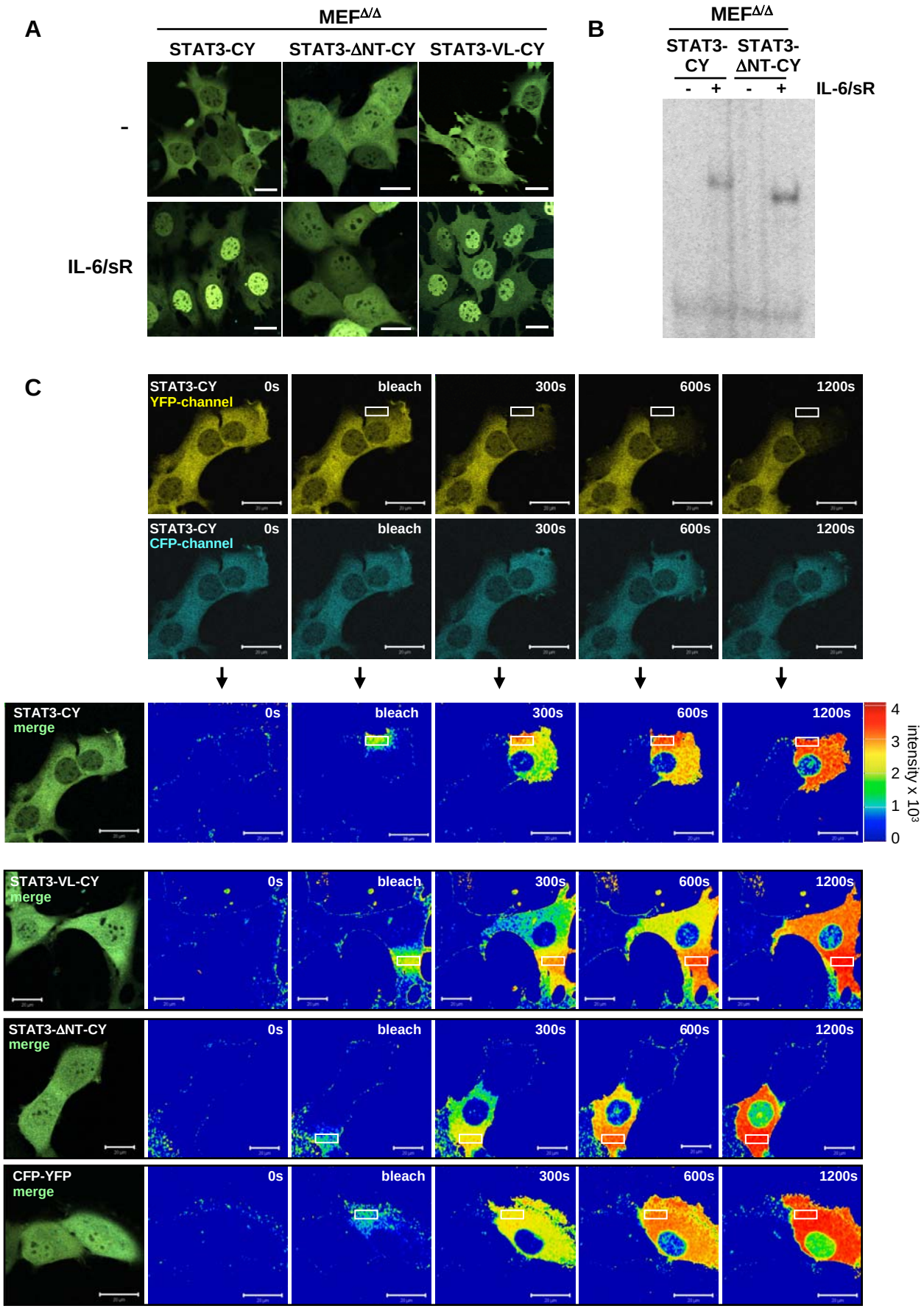

Vogt et al. Fig. 6

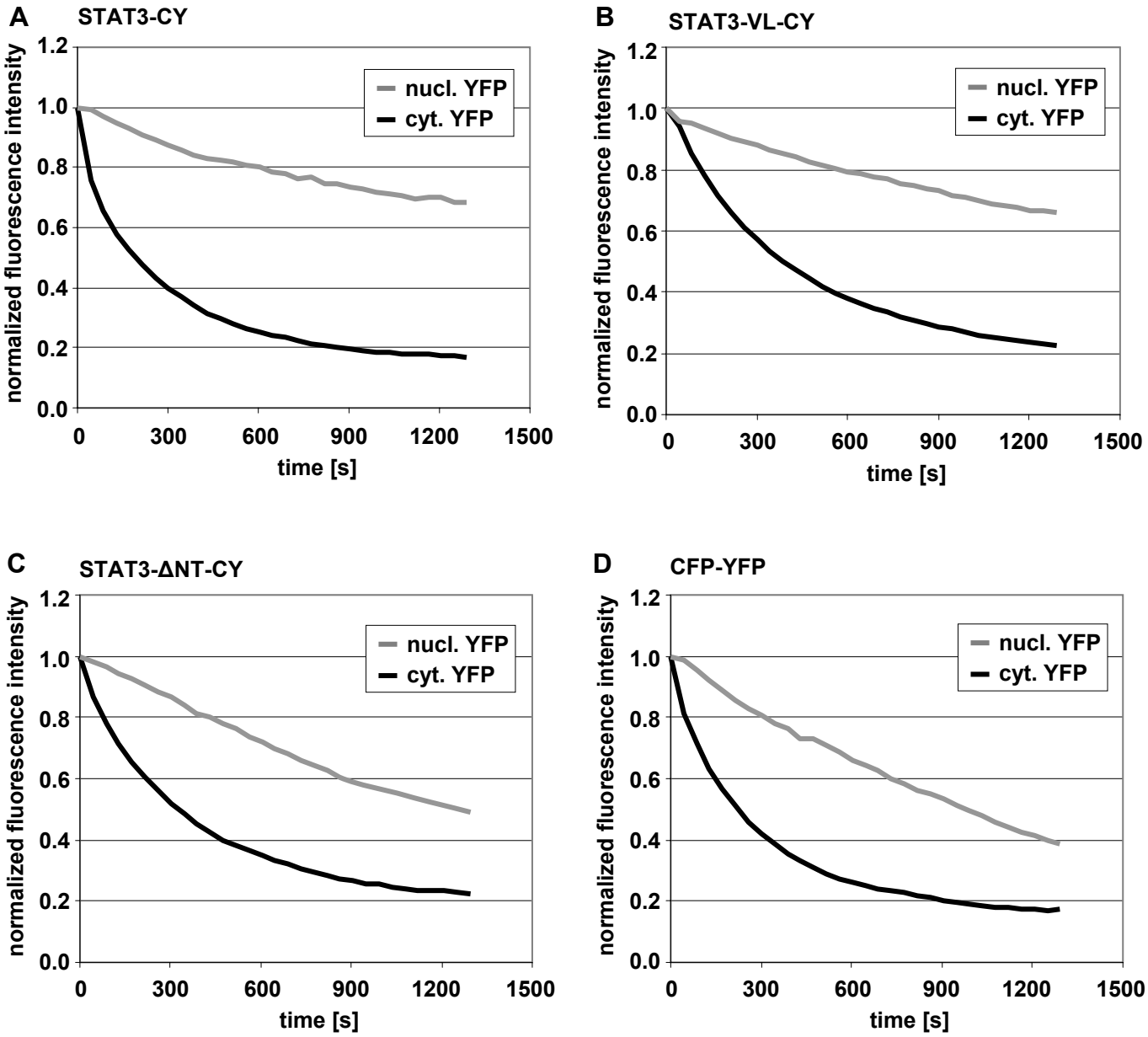

Vogt et al. Fig. 7

Table 1: Diffusion coefficients and average molecular masses derived from 2f-FCS experiments. n: total number of measurements from three independent samples per construct. The predicted molecular masses have been calculated from the known amino acid sequences of the proteins.

	n	Diffusion coefficient	Hydrodynamic radius	Average molecular mass	Predicted molecular mass
		$\times 10^{-6}$ cm^2 x s^{-1}	nm	kDa	kDa
eGFP	3	1.03 ± 0.04	2.4 ± 0.1		27
STAT3-eGFP	12	0.54 ± 0.08	4.6 ± 0.8	216 ± 99	236 (dimer)
STAT3-ΔNT-eGFP	10	0.70 ± 0.03	3.5 ± 0.2	88 ± 11	99 (monomer)